

Electron momentum spectroscopy study on trifluorobromomethane: Electronic structure and electron correlation

Guangqing Chen(陈广庆), Shanshan Niu(牛珊珊), Yanguo Tang(唐亚国), Yuting Zhang(张雨亭), Zhaohui Liu(刘朝辉), Chunkai Xu(徐春凯), Enliang Wang(王恩亮), Xu Shan(单旭), and Xiangjun Chen(陈向军)

Citation: Chin. Phys. B, 2025, 34 (**4**): 043401. DOI: 10.1088/1674-1056/adb273
Journal homepage: http://cpb.iphy.ac.cn; http://iopscience.iop.org/cpb

What follows is a list of articles you may be interested in

Atomic structure and collision dynamics with highly charged ions

Xinwen Ma(马新文), Shaofeng Zhang(张少锋), Weiqiang Wen(汶伟强), Zhongkui Huang(黄忠魁), Zhimin Hu(胡智民), Dalong Guo(郭大龙), Junwen Gao(高俊文), Bennaceur Najjari, Shenyue Xu(许慎跃), Shuncheng Yan(闫顺成), Ke Yao(姚科), Ruitian Zhang(张瑞田), Yong Gao(高永), and Xiaolong Zhu(朱小龙)

Chin. Phys. B, 2022, 31 (**9**): 093401. DOI: 10.1088/1674-1056/ac8736

Vibrational effects on electron momentum distributionsof outer valence orbitals of benzene

Yu Zhang(张钰), Shanshan Niu(牛珊珊), Yaguo Tang(唐亚国), Yichun Wang(王忆纯), Xu Shan(单旭), Xiangjun Chen(陈向军)

Chin. Phys. B, 2020, 29 (**2**): 023402. DOI: 10.1088/1674-1056/ab671b

Influence of electron correlations on double-capture process in proton helium collisions

Hoda Ghavaminia, Ebrahim Ghanbari-Adivi

Chin. Phys. B, 2015, 24 (**7**): 073401. DOI: 10.1088/1674-1056/24/7/073401

Projectile angular-differential cross sections for single electron transfer in fast He^{+}-He collisions

Ebrahim Ghanbari-Adivi, Hoda Ghavaminia

Chin. Phys. B, 2015, 24 (**3**): 033401. DOI: 10.1088/1674-1056/24/3/033401

Assessment of delocalized and localized molecular orbitals through electron momentum spectroscopy

Liu Yuan (刘源), Cheung Ling-Fung (张凌峰), Ning Chuan-Gang (宁传刚)

Chin. Phys. B, 2014, 23 (**6**): 063403. DOI: 10.1088/1674-1056/23/6/063403

Electron momentum spectroscopy study on trifluorobromomethane: Electronic structure and electron correlation

Guangqing Chen(陈广庆), Shanshan Niu(牛珊珊), Yaguo Tang(唐亚国), Yuting Zhang(张雨亭), Zhaohui Liu(刘朝辉), Chunkai Xu(徐春凯), Enliang Wang(王恩亮), Xu Shan(单旭)†, and Xiangjun Chen(陈向军)

Hefei National Research Center for Physical Sciences at the Microscale and Department of Modern Physics, University of Science and Technology of China, Hefei 230026, *China*

(Received 14 January 2025; revised manuscript received 23 January 2025; accepted manuscript online 5 February 2025)

We present a comprehensive electron momentum spectroscopy study on the electronic structure of trifluorobromomethane. The binding energy spectrum and electron momentum profiles of the entire outer-valence orbitals and the first inner-valence orbital along with several shake-up states were measured by using a high-sensitivity (e, 2e) apparatus at an electron impact energy of 1213 eV. Theoretical calculations employing the density functional theory with B3LYP hybrid functional and the symmetry-adapted cluster configuration-interaction method were performed to interpret the experimental results. Important effects of electron correlations in the initial neutral and final ionic states on the electron momentum profiles have been observed.

Keywords: electron momentum spectroscopy, electronic structure, electron correlation

PACS: 34.80.Gs, 31.15.ae, 31.15.V–

DOI: 10.1088/1674-1056/adb273 **CSTR:** 32038.14.CPB.adb273

1. Introduction

Trifluorobromomethane (CF_3Br) has historically been employed as an efficient fire suppressant throughout the last century due to its high inhibition efficiency.[1,2] Despite being phased out under the Montreal protocol because of its significant contribution to stratospheric ozone depletion, CF_3Br continues to serve as a critical benchmark for evaluating alternative fire suppressants.[3] Understanding its inhibitory mechanisms is therefore essential for establishing a baseline to compare the effectiveness of other candidate fire suppressants.

Fundamental studies[3–6] have indicated that CF_3Br competes effectively with the chain branching reactions in combustion, particularly the reaction $H + O_2 \rightleftarrows O + OH$. This inhibitory action is driven by the release of reactive intermediates, such as bromine (Br) atoms and CF_3 radicals. The molecular structure of CF_3Br, featuring a relatively weak C–Br bond and stronger C–F bonds, facilitates the release of Br during combustion. Bromine atoms react with hydrogen radicals to form hydrogen bromide (HBr), which scavenges H radicals, thereby slowing down combustion by promoting the formation of less-reactive hydrogen molecules (H_2). Furthermore, the presence of fluorine atoms in the CF_3 radical enhances CF_3Br's ability to permanently remove H radicals,[4] making it more effective as a fire suppressant than other brominated compounds, such as HBr or CH_3Br.

The flame-suppressing efficiency of CF_3Br is intimately related to its electronic structure, particularly the distribution of electron density around the Br and CF_3 groups. Detailed analysis of its electronic structure not only offers valuable insights into the mechanisms underlying its flame suppression capabilities, but also provides guidelines for next-generation fire suppressants. The ionization potentials of CF_3Br were intensively studied using photoelectron spectroscopy (PES) with He I, He II, and synchrotron radiation sources.[7–12] The dependence of the photoionization cross sections or photoelectron asymmetry parameters on the photon energies were also investigated and used to analyze the orbital characteristics of CF_3Br.[9–11] Electron momentum spectroscopy (EMS),[13–17] also referred to as binary (e, 2e) spectroscopy, is another powerful technique that not only provides ionization energies but also directly measures the spherically averaged electronic density distributions in momentum space for individual atomic and molecular orbitals. Over the past decades, EMS has proven its unique ability in investigating electronic structures of atoms and molecules.[13,16–27] For CF_3Br, Wu *et al*. investigated electron localized feature of the highest occupied molecular orbital (HOMO) using EMS technique in the wavefunction domain[28] but did not refer to other molecular orbitals of CF_3Br.

In this study, we present a detailed EMS study on CF_3Br by a high-sensitivity (e, 2e) apparatus operating at an incident energy of 1200 eV plus the binding energy. Detailed specifications of the spectrometer have been reported elsewhere.[29] The instrumental energy and momentum resolution were es-

†Corresponding author. E-mail: xshan@ustc.edu.cn

© 2025 Chinese Physical Society and IOP Publishing Ltd. All rights, including for text and data mining, AI training, and similar technologies, are reserved.

timated to be 1.1 eV (FWHM) and 0.15 a.u. based on measurements of Ar 3p ionization, respectively. The experimental electron momentum profiles of CF_3Br for the whole outer-valence orbitals and the first inner-valence orbital along with several satellites have been obtained, which are compared with theoretical calculations performed by density functional theory (DFT-B3LYP)[30,31] and the symmetry-adapted cluster configuration-interaction (SAC-CI) method,[32] both utilizing the augmented correlation-consistent-polarized valence triple-zeta (aug-cc-pVTZ) basis set.[33]

2. Experimental and theoretical background

EMS relies on the kinematically complete (e, 2e) reaction in which an orbital electron from the target atom or molecule is ejected by a high-energy incident electron collision. This electron impact ionization process can be expressed as

$$\mathrm{e_i}\left(E_\mathrm{i},\boldsymbol{p}_\mathrm{i}\right)+\mathrm{T}\rightarrow\mathrm{T^+}+\mathrm{e_s}\left(E_\mathrm{s},\boldsymbol{p}_\mathrm{s}\right)+\mathrm{e_e}\left(E_\mathrm{e},\boldsymbol{p}_\mathrm{e}\right), \tag{1}$$

where the subscripts i, s, and e denote the energy E and momenta $\boldsymbol{p}$ of the incident, scattered, and ejected electrons, respectively. The target atom or molecule is denoted as T, with $\mathrm{T^+}$ representing the residual ion. Within the binary-encounter approximation, the electron impact ionization is treated as a direct collision between the incident and target electrons. The binding energy ε_f and the momentum $\boldsymbol{p}$ of the orbital electron in the target can be obtained using the conservation laws of energy and momentum

$$\varepsilon_\mathrm{f}=E_\mathrm{i}-E_\mathrm{s}-E_\mathrm{e}, \tag{2}$$

$$\boldsymbol{p}=\boldsymbol{p}_\mathrm{s}+\boldsymbol{p}_\mathrm{e}-\boldsymbol{p}_\mathrm{i}. \tag{3}$$

The high-sensitivity EMS spectrometer[29] was employed for the present study on CF_3Br. In brief, an electron from the target gaseous CF_3Br molecule is ejected by an incident electron with energy of 1213 eV. The scattered and ejected electrons, which have equal energies ($E_\mathrm{s}=E_\mathrm{e}$) and equal polar angles ($\theta_\mathrm{s}=\theta_\mathrm{e}=45^\circ$) relative to the incident electron direction, are initially decelerated by retarding lenses, then energy-dispersed by a 90° sector spherical electrostatic analyzer, and ultimately detected by a position-sensitive detector (PSD) consisting of a pair of micro-channel plates (MCPs) arranged in a chevron configuration followed by a delay-line anode.[34] Under non-coplanar symmetric kinematic arrangement, the magnitude of target orbital electron momentum is given by

$$p=\sqrt{\left(p_0-2p_1\cos 45^\circ\right)^2+\left[2p_1\sin 45^\circ\sin\left(\frac{\phi}{2}\right)\right]^2}, \tag{4}$$

where ϕ is the relative azimuthal angle between the scattered and ejected electrons.

On the theoretical side, the plane wave impulse approximation (PWIA)[15] is usually employed in EMS. This approximation assumes that the energies of both the incident and outgoing electrons are sufficiently high, allowing them to be accurately described by plane waves. The triple differential cross section (TDCS) for a gaseous target is given by

$$\frac{\mathrm{d}^3\sigma}{\mathrm{d}\Omega_1\,\mathrm{d}\Omega_2\,\mathrm{d}E_1}\propto\frac{1}{4\pi}\int\mathrm{d}\Omega\left|\langle\boldsymbol{p}\Psi_\mathrm{f}^{(N-1)}|\Psi_\mathrm{i}^{N}\rangle\right|^2, \tag{5}$$

where $\boldsymbol{p}$ represents the plane wave associated with the knocked-out electron from the target, while $\Psi_\mathrm{f}^{(N-1)}$ and Ψ_i^{N} denote the total electronic wavefunctions of the final ionic state with $N-1$ electrons and the initial ground state with N electrons, respectively. The integral over 4π accounts for the spherical averaging resulting from the random orientation of gaseous targets. The TDCS is proportional to the square of the overlap between the initial and final states (referred to as the Dyson orbital). Under the weak coupling approximation,[15] the overlap can further be described as

$$\langle\boldsymbol{p}\Psi_\mathrm{f}^{N-1}|\Psi_\mathrm{i}^{N}\rangle=\left(S_\mathrm{f}^{\alpha}\right)^{1/2}\varphi_\alpha\left(\boldsymbol{p}\right), \tag{6}$$

where S_f^{α} denotes the pole strength, representing the probability of a single-hole configuration in the final ion state, and $\varphi_\alpha(\boldsymbol{p})$ is the normalized one-electron Dyson orbital which can be approximated by the Hartree–Fock (HF)[13] or Kohn–Sham (KS) orbitals.[35] The TDCS then simplifies to

$$\frac{\mathrm{d}^3\sigma}{\mathrm{d}\Omega_1\,\mathrm{d}\Omega_2\,\mathrm{d}E_1}\propto\frac{1}{4\pi}S_\mathrm{f}^{\alpha}\int\mathrm{d}\Omega\left|\varphi_\alpha^{\mathrm{HF\ or\ KS}}\left(\boldsymbol{p}\right)\right|^2, \tag{7}$$

where the integral is called as the spherically averaged electron momentum profile.

It is noted that HF and B3LYP approaches only consider the electron correlation in the ground state of neutral molecule. To further consider the electron correlations in the final states, the CI or SAC–CI methods are required. In the SAC–CI theory, the SAC wavefunction is used to describe the ground state, while the SAC–CI wavefunction is applied to the final states. For a closed-shell singlet ground state, the wavefunction is described as the SAC expansion by

$$\left|\Psi_0^{\mathrm{SAC}}\right\rangle=\left(1+\sum_I C_I S_I+\frac{1}{2}\sum_{I,J}C_I C_J S_I S_J+\cdots\right)|0\rangle, \tag{8}$$

where $|0\rangle$ is the HF determinant of the ground state, C is the coefficient, and S denotes the symmetry-adapted excitation operator. For the final state, the SAC–CI wavefunction is obtained by modifying the SAC wavefunction of the ground state, which is typically written as

$$\left|\Psi_\mathrm{f}^{\mathrm{SAC-CI}}\right\rangle=\Re\left|\Psi_0^{\mathrm{SAC}}\right\rangle. \tag{9}$$

Here, $\Re=\sum_k d_k R_k$ is the excitation operation, with R_k representing excitation, ionization, or electron-attached operators, and d_k the corresponding coefficients.

The Dyson orbital, calculated using SAC–CI theory, is a linear combination of orthogonal HF orbitals,

$$\Psi_{\text{Dyson}} = \left\langle \Psi_{\text{f}}^{\text{SAC-CI}} \middle| \Psi_0^{\text{SAC}} \right\rangle = \sum_j c_j \varphi_j^{\text{HF}}, \tag{10}$$

where φ_j^{HF} are the HF orbitals and c_j are the corresponding coefficients. The PS of the Dyson orbital is given by $S_{\text{f}} = \sum_j c_j^2$.

In the present calculations, the equilibrium molecular geometry of CF_3Br in its ground state is optimized using the B3LYP method with aug-cc-pVTZ basis set. The wavefunctions in position space are calculated under the optimized equilibrium geometry of molecules by employing both the B3LYP and SAC–CI general-*R* methods with the same basis set. The corresponding momentum-space wavefunctions are obtained by Fourier transformation, and the electron momentum profiles are therefore calculated by B3LYP and SAC–CI approaches according to Eqs. (7) and (10), respectively. Additionally, the SAC–CI general-*R* method has also been used to calculate the ionization potentials (IPs) and pole strengths (PSs) for main transition and satellite states, enabling the construction of simulated binding energy spectra for CF_3Br. Detailed information on the IPs and PS values is summarized in Table 1, alongside experimental IP values from EMS and PES for comparison. All above theoretical calculations are performed using the GAUSSIAN 09 program suite.[36]

Table 1. SAC–CI calculated ionization potentials (IPs), pole strengths (PSs), and main configurations of the ionized states of CF_3Br and the corresponding experimental IPs from present EMS and previous PES studies.

MO	SAC–CI general-R[a]			EMS[a]	PES[b]	PES[c]
	IP (eV)	PS	Main configurations ($\|c\| \geq 0.1$)	IP (eV)		
5e	11.71	0.841	$0.96(5e^{-1})$	12.1	12.08	12.08
$5a_1$	13.79	0.838	$0.96(5a_1^{-1})$	14.3	14.28	14.28
$1a_2$	15.77	0.820	$0.96(1a_2^{-1})$	15.8	15.86	15.86
4e	16.27	0.820	$0.95(4e^{-1})$	16.5	16.55	16.55
3e	17.33	0.817	$0.95(3e^{-1})$	17.6	17.57	17.57
$4a_1$	19.64	0.800	$0.94(4a_1^{-1}) + 0.12(5a_1^{-1})$	20.0	19.8	19.8
2e	20.90	0.813	$0.96(2e^{-1})$	21.1	20.9	20.9
	22.51	0.182	$0.38(3a_1^{-1}) - 0.24(2a_1^{-1}) - 0.41(5e^{-1}9a_15e^{-1})$	22.6		
$3a_1$	23.81	0.632	$0.85(3a_1^{-1}) - 0.20(5e^{-1}9a_15e^{-1})$	23.8	23.7	23.7
$2a_1$	25.73	0.443	$0.68(2a_1^{-1}) + 0.19(3a_1^{-1}) - 0.23(4e^{-1}9a_15e^{-1})$	25.5		25.0
	26.13	0.055	$0.24(2a_1^{-1}) - 0.51(4e^{-1}9a_15e^{-1}) - 0.46(4e^{-1}6e5e^{-1}) - 0.44(4e^{-1}9a_15e^{-1})$			
	26.77	0.030	$0.18(2a_1^{-1}) + 0.46(5a_1^{-1}9a_15a_1^{-1})$			
	27.22	0.021	$0.15(2a_1^{-1}) - 0.45(5e^{-1}11a_15e^{-1})$			
	28.21	0.023	$0.16(2a_1^{-1}) - 0.34(5e^{-1}6a_15e^{-1})$	28.0		
	30.86	0.012	$0.10(2a_1^{-1}) + 0.34(4e^{-1}11a_15e^{-1})$			
	30.99	0.011	$0.10(2a_1^{-1}) + 0.29(4e^{-1}11a_15e^{-1})$			
	31.10	0.010	$0.10(2a_1^{-1}) + 0.27(4e^{-1}6a_15e^{-1})$			
	31.21	0.016	$0.12(2a_1^{-1}) - 0.28(5e^{-1}8a_15a_1^{-1})$			
	31.28	0.010	$0.10(2a_1^{-1}) - 0.30(5e^{-1}6a_14e^{-1})$			

[a] Present work, [b] Ref. [9], [c] Ref. [11].

3. Results and discussion

CF_3Br contains 68 electrons and exhibits C_{3v} symmetry. Its ground state electronic configuration can be described using B3LYP/aug-cc-pVTZ as

$$(\text{core})^{36}\underbrace{(1a_1)^2(1e)^4(2a_1)^2}_{\text{inner-valence}}\underbrace{(3a_1)^2(2e)^4(4a_1)^2(3e)^4(4e)^4(1a_2)^2(5a_1)^2(5e)^4}_{\text{outer-valence}}.$$

The valence shell comprises eleven orbitals, which can be categorized into two groups: eight outer-valence orbitals and three inner-valence orbitals. The calculated energy ordering of these valence orbitals aligns well with the sequence established by previous PES experiments.[9–11] The experimentally obtained two-dimensional (2D) density map of CF_3Br, as shown in Fig. 1(a), illustrates the TDCS dependent on orbital electron binding energy and the relative azimuthal angle ϕ between two outgoing electrons (i.e., orbital electron momentum according to Eq. (4)). This 2D map offers detailed information of electron momentum distribution, binding energy, and orbital symmetry.

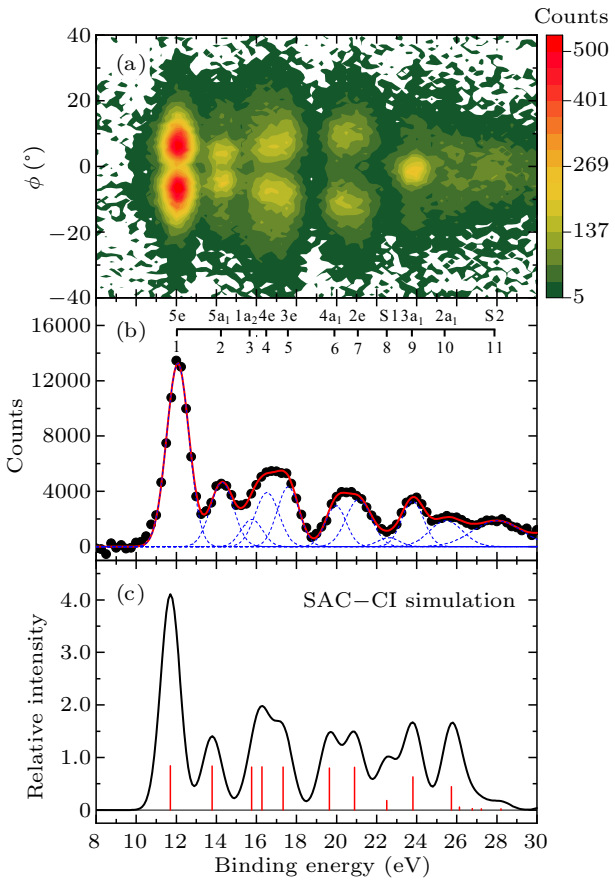


Fig. 1. (a) The 2D density map on electron binding energy and momentum (i.e., ϕ). (b) Total binding energy spectrum. The dashed lines represent Gaussian functions used to fit BES and the solid line is the sum of them. (c) SAC–CI simulated binding energy spectrum. Positions and heights of the vertical bars indicate the calculated IPs and PSs of the relevant transitions.

3.1. Binding energy spectrum

The experimental binding energy spectrum (BES) of CF_3Br, spanning 8 eV to 30 eV, was obtained by integrating the 2D map across all relative azimuthal angles, as depicted in Fig. 1(b). The BES reveals seven distinct features, including five well-resolved envelopes in a range of the 8 eV–25 eV and two relatively weaker envelopes in the range of 25 eV–30 eV. CF_3Br has been extensively studied by PES,[7,9–11] which enables the assignment of nine orbitals, encompassing all outer-valence orbitals and the first inner-valence orbital $2a_1$. In the experimental BES, eleven Gaussian peaks are employed to identify the contributions from each main ionic state and its corresponding shake-up states, as shown by dashed blue lines and the solid red line represents their sum. The positions of most peaks are primarily referred to the vertical ionization potentials reported in earlier work of PES,[11] while their widths are obtained by the convolution of Franck–Condon widths and our instrumental energy resolution of 1.1 eV (FWHM). Additionally, peak 8 and peak 11 are introduced to account for the shake-up states located at the foot of the main states $3a_1$ and $2a_1$ under the guidance of the SAC–CI general-*R* calculation. Molecular orbitals corresponding to Gaussian peaks are illustrated at the top of Fig. 1(b), with vertical lines marking their ionization energies.

In the outer-valence region, peak 1 arises from the ionization of the highest occupied molecular orbital (HOMO) 5e, which has the highest intensity and is well resolved in the BES. This broad peak contains two unresolved components ($5e_{1/2}$, $5e_{3/2}$) due to spin-orbit coupling effect.[9] Peak 2 stands for the next highest occupied molecular orbital $5a_1$. The envelope in the energy range of about 15 eV to 19 eV includes three unresolved peaks (peaks 3–5), corresponding to the ionization of molecular orbitals $1a_2$, 4e, and 3e, respectively. The next envelope in the energy range of about 19 eV to 23 eV includes two unresolved peaks (peak 6 and peak 7), which refers to the orbital $4a_1$ and 2e, respectively. Peak 9 is attributed solely to the orbital $3a_1$. In the inner-valence region, only the first orbital $2a_1$ is resolved (peak 10) while other inner-valence orbitals (1e and $1a_1$) are located at binding energy much larger than 30 eV as supported by synchrotron radiation PES work.[10] Peak 8 and peak 11 represent satellite states associated with the $3a_1$ and $2a_1$ ionizations.

For the sake of comparison, the synthesized theoretical BES constructed using SAC–CI general-*R* calculation is presented in Fig. 1(c). In the simulation, Gaussian functions are used to represent each transition. Their widths are matched by the instrumental energy resolution and their positions are the calculated IPs, while their intensities (i.e., areas) are simply the product of the electron densities and PSs. The theoretical BES closely matches the experimental spectrum, accurately capturing its key features and thereby further validating the theoretical model.

3.2. Electron momentum profiles

The experimental electron momentum profiles (XMPs) were obtained by plotting the fitted areas of corresponding Gaussian peaks in the BES against the orbital electron momentum p, which was derived from the relative azimuthal angles ϕ using Eq. (4). Theoretical electron momentum profiles (TMPs) were calculated using the B3LYP and SAC–CI methods with aug-cc-pVTZ basis set at the optimized equilibrium geometry. To facilitate direct comparison, the TMPs were convoluted with the instrumental angular resolution using the Gaussian-weighted planar grid (GWPG)[37] method. The normalization factor between the XMPs and the TMPs was determined by matching the TMP and XMP of the HOMO (5e orbital). Figures 2–7 illustrate the results of momentum profiles for all outer-valence orbitals and the first inner-valence orbital along with several satellite states. Additionally, molecular orbital maps in position space calculated by B3LYP/aug-cc-pVTZ are also inserted in the graph, which visually depict the electron wavefunctions, with blue and yellow indicating opposite phases.

As shown in Fig. 2, the XMP of the HOMO 5e orbital exhibits a characteristic p-type profile, with a peak at $p \sim 0.5$ a.u. The TMPs obtained from the B3LYP and SAC–CI calculations

provide an excellent description of the XMP, demonstrating the reliability of these computational approaches. The molecular orbital map reveals that the 5e orbital can be attributed mainly to bromine localized lone pair orbitals with substantial Br(4p) character. This finding aligns with a previous EMS research by Wu *et al.*,[28] which showed that the momentum distribution of the HOMO 5e orbital is nearly identical to that of the 4p orbital in a free Br atom.

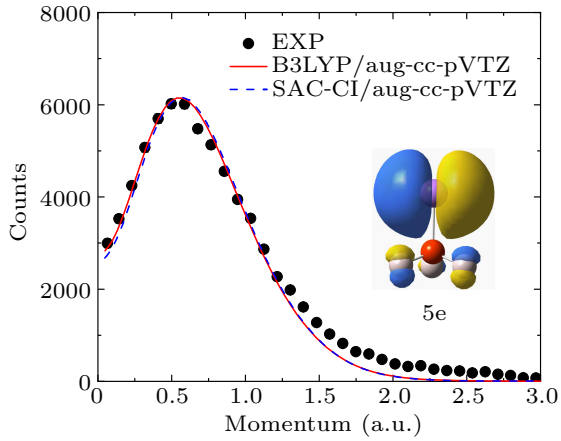


Fig. 2. The XMP and TMPs for 5e orbital of CF_3Br. The solid and dash lines correspond to B3LYP/aug-cc-pVTZ and SAC–CI/aug-cc-pVTZ calculations, respectively. The orbital map calculated by B3LYP/aug-cc-pVTZ is shown in the graph.

The XMP for $5a_1$ orbital is shown in Fig. 3, exhibiting two distinct maxima at $p \sim 0.3$ a.u. and $p \sim 1.2$ a.u. The molecular orbital map displays a predominant C–Br σ bonding character, in accordance with the identification in the PES works.[11] This bonding orbital primarily arises from the contribution of C($2p_z$) and Br($4p_z$) atomic orbitals. Additionally, minor F(2p) components of three fluorine atoms are also engaged in this orbital. This composition provides a plausible explanation for the p-type character and the observed dual maxima in its XMP. As shown in Fig. 3, the B3LYP calculation offers better agreement with the experiment than the SAC–CI calculation, revealing the significance of electron correlations in the initial state.

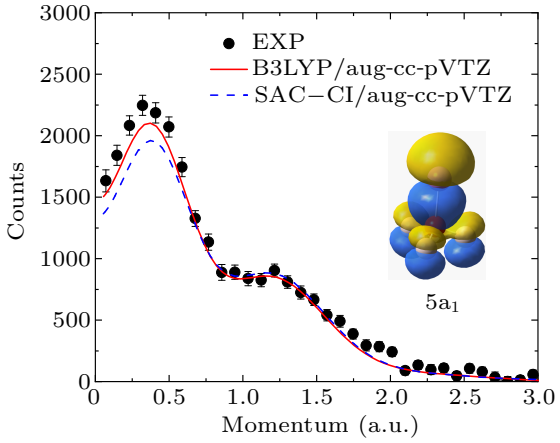


Fig. 3. The same as that of Fig. 2, but for $5a_1$ orbital.

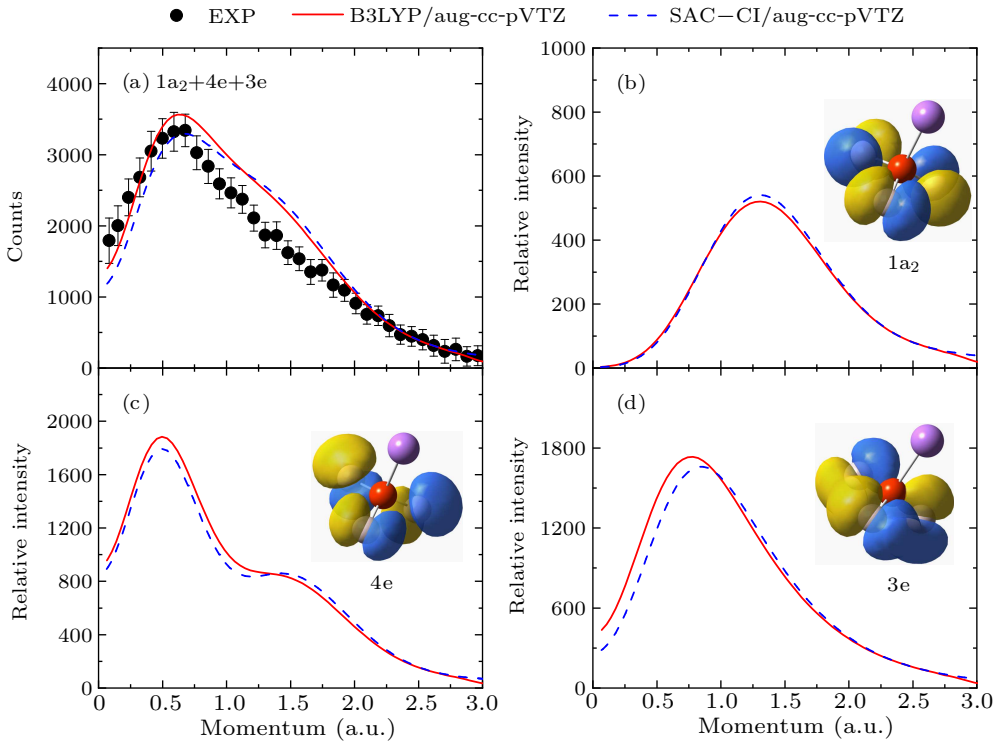


Fig. 4. (a) The summed XMP and TMPs for $1a_2$, 4e, and 3e orbitals. (b), (c), and (d) represent the TMPs and orbital maps for (b) $1a_2$, (c) 4e, and (d) 3e, respectively.

The next three orbitals of $1a_2$, 4e, and 3e primarily originate from fluorine lone pair electrons, as the orbital maps showed in Fig. 4. Different spatial configurations of fluorine lone pair for these orbitals make their TMPs different, i.e., a maximum at $p \sim 1.3$ a.u. for $1a_2$, two maxima at $p \sim 0.5$ a.u. and 1.5 a.u. for 4e and one maximum at $p \sim 0.7$ a.u. for 3e. In

the present experiment, the ionization bands of these orbitals cannot be separated. The uncertainty from the deconvolution of BES is too large to obtain the reliable XMP for individual orbital. So only the summed XMP together with the TMPs for these orbitals are presented in Fig. 4(a). Although there is a visible discrepancy, an overall agreement of the TMPs with the XMP can be seen from the figure. Recent works[39–41] showed that molecular vibration and distorted wave effects play an obvious role in improving the difference between theory and experiment. To analyze the reasons resulted in the discrepancy specifically, further high-level calculations are demanded to consider more physical factors and high-resolution experiment is also expected to separate these three orbitals in future work.

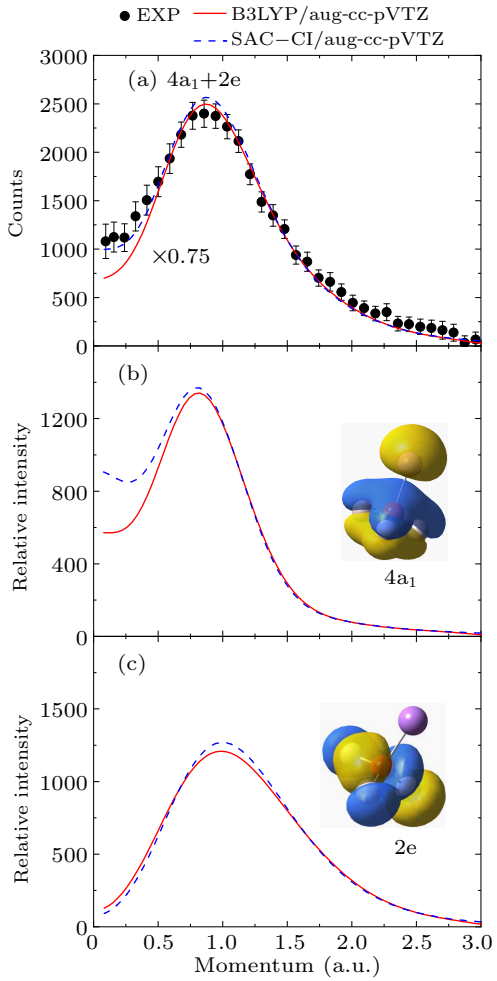


Fig. 5. (a) The summed XMP and TMPs for $4a_1$ and 2e orbitals. (b) and (c) represent the TMPs and orbital maps for individual $4a_1$ and 2e, respectively.

Figure 5 shows the experimental and theoretical results for $4a_1$ and 2e orbitals. The calculated orbital maps illustrate that these two orbitals are dominantly C–F σ bonding characters. The additional C–Br anti-bonding component for $4a_1$ orbital leads to its TMP different from that of 2e orbital, particularly to the intensity at low momentum region. The SAC–CI calculation shows that the final state of $4a_1$ ionization also includes a little contribution of $5a_1$ ionic state, which makes an obvious "turn up" intensity of the TMP appear at low momentum region as Fig. 5(b) showed. The ionization bands of $4a_1$ and 2e orbitals are not resolved duo to the poor energy resolution. Only the summed XMP for these two orbitals are plotted and compared with the corresponding TMPs in Fig. 5(a). The XMP exhibits a p-type character with a maximum located at $p \sim 0.8$ a.u. except for a remarkable intensity at the origin of momentum. When the TMPs multiplied by a factor of 0.75, the TMPs calculated by B3LYP and SAC–CI approaches generally agree with the XMP. This factor indicates the pole strength of ionizations from $4a_1$ and 2e orbitals. The SAC–CI calculation provides better description on the XMP's intensity at low momentum than the B3LYP calculation, revealing the role of configuration interaction in the final state.

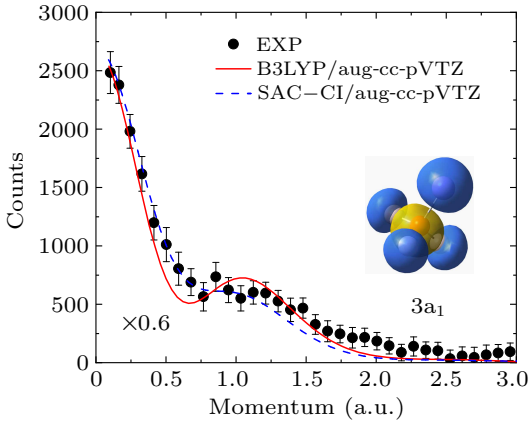


Fig. 6. The summed XMP and TMPs for $3a_1$ and its satellite.

The $3a_1$ is the last outer-valence orbital, whose orbital map depicts a C–Br and C–F σ anti-bonding character. The SAC–CI calculation predicts the ionization potential of this orbital at 23.81 eV, agreeing with present EMS and previous PES measurements. Besides, a very weak satellite state at 22.51 eV accompanying the ionization is also predicted. Considering large uncertainty in deriving the XMP for this satellite, an additive XMP for main state and this satellite state are presented in Fig. 6, along with the TMPs for comparison. The XMP shows a mixed sp-type character. The TMPs multiplied by a factor of 0.6 agree with the XMP well. This factor represents the pole strength from $3a_1$ ionization contributed to this energy region, which is in accordance with the SAC–CI prediction. The SAC–CI calculation offers a more accurate description of the XMP's intensity in the momentum range from 0.25 a.u. to 1.25 a.u. compared to the B3LYP calculation, highlighting the significance of configuration interaction in the final state.

The observed ionization peak at about 25.5 eV in BES corresponds to the first inner-valence orbital $2a_1$ and the peak around 28 eV is contributed from many satellite states associating with the ionization of $2a_1$, according to the present

SAC–CI predictions. To account for these satellites in the experimental BES, Gaussian peak 11 centered at 28.0 eV has been introduced to deduce the XMP, as shown in Fig. 1(b). The XMPs for $2a_1$ main state and satellites are presented in Fig. 7, along with the TMPs for comparison. The SAC–CI calculation well predicts the XMP's shape and can reproduce the experiment as it is multiplied by a factor of 0.24, but the B3LYP calculation cannot. It is easily understandable that the B3LYP is based on one-electron picture while the SAC–CI involves multi-electron process to consider shake-up excitations accompanying ionization. This is further supported by the configuration components of the final ion state listed in Table 1. The configuration mixture of the $2a_1$ and $3a_1$ states as well as the shake-up states during ionization should be responsible for the present observation on the XMP. Figure 7(b) shows the XMP for the satellites, where the TMP covers the cooperative contributions of serval satellite states predicted by SAC–CI calculation. One can see that a general agreement is visible between the XMP and the TMP multiplied by a factor of 0.28. The factors obtained via comparing TMP with XMP represent the reassignment of the ionization pole strengths to different ionic final states, which means that smaller the PS value, in some extent, stronger electron correlation in the final states.

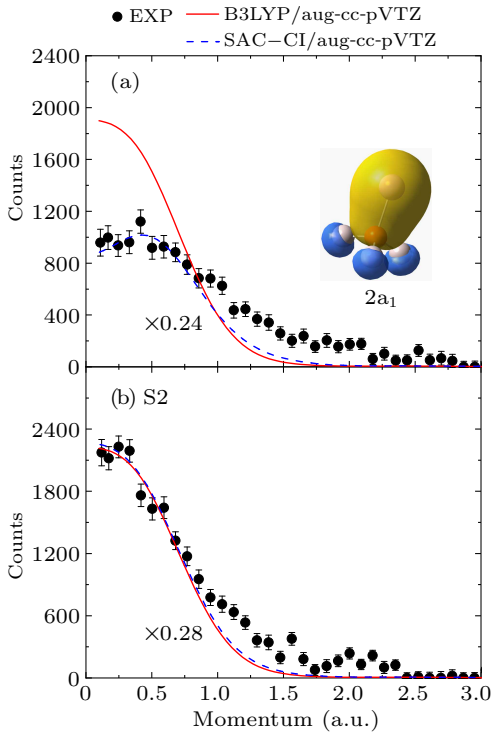


Fig. 7. The XMPs and TMPs for (a) $2a_1$ and (b) its satellites.

4. Summary

The experimental and theoretical EMS studies on the electronic structure of CF_3Br have been carried out in the present work. The BES and XMPs for the entire outer-valence orbitals and the first inner-valence orbital along with several satellite states have been obtained and compared with the theoretical calculations by the B3LYP/aug-cc-pVTZ and SAC–CI/aug-cc-pVTZ methods. The XMP for HOMO 5e was found to exhibit atomic orbital-like characteristics, closely resembling to the 4p of a free Br atom. For C–Br σ bonding orbital $5a_1$, the B3LYP calculation describes the XMP better than the SAC–CI calculation, revealing the significance of electron correlations in the initial state. While for $4a_1$, $3a_1$, and $2a_1$ orbitals, the SAC–CI calculation better reproduces the XMP than the B3LYP approach exhibiting significant influence of electron correlations in the final states. These findings provide more insights into the valence orbital electron properties of CF_3Br and will be helpful to understand its flame suppression mechanisms.

Acknowledgement

Project supported by the National Natural Science Foundation of China (Grant No. 12127804).

References

[1] Gann R G 1975 *Halogenated Fire Suppressants* (Washington, D.C.: American Chemical Society) p. 1
[2] Miziolek A W and Tsang W 1995 *Halon Replacements: Technology and Science* (Washington, DC: American Chemical Society) p. 1
[3] Casias C R and Thomas McKinnon J 1998 *Symp. (Int.) Combust.* **27** 2731
[4] Westbrook C K 1983 *Combust. Sci. Technol.* **34** 201
[5] Noto T, Babushok V, Burgess D R, Hamins A, Tsang W and Miiolek A 1996 *Symp. (Int.) Combust.* **26** 1377
[6] Osorio C H, Vissotski A J, Petersen E L and Mannan M S 2013 *Combust. Flame* **160** 1044
[7] Doucet J, Sauvageau P and Sandorfy C 1973 *J. Chem. Phys.* **58** 3708
[8] Doucet J, Gilbert R, Sauvageau P and Sandorfy C 1975 *J. Chem. Phys.* **62** 366
[9] Cvitaš T, Güsten H, Klasinc L, Novadj I and Vančik H 1977 *Z. Naturforsch. A* **32** 1528
[10] Novak I, Benson J M and Potts A W 1986 *Chem. Phys.* **104** 153
[11] Bozek J D, Bancro G M, Cutler J N, Tan K H, Yates B W and Tse J S 1989 *Chem. Phys.* **132** 257
[12] Johnson J, Cutler J N, Bancroft G M, Hu Y F and Tan K H 1997 *J. Phys. B: At., Mol. Opt. Phys.* **30** 4899
[13] McCarthy I E and Weigold E 1991 *Rep. Prog. Phys.* **54** 789
[14] Brion C E 1986 *Int. J. Quantum Chem.* **29** 1397
[15] Coplan M A, Moore J H and Doering J P 1994 *Rev. Mod. Phys.* **66** 985
[16] Takahashi M 2009 *Bull. Chem. Soc. Jpn.* **82** 751
[17] Ren X G, Ning C G, Deng J K, Zhang S F, Su G L, Huang F and Li G Q 2005 *Phys. Rev. Lett.* **94** 163201
[18] Niu S S, Tang Y G, Liu Z H, Shi Y F, Wang E L, Shan X and Chen X J 2019 *Phys. Rev. A* **99** 022512
[19] Huang C W, Shan X, Zhang Z, Wang E L, Li Z J and Chen X J 2010 *J. Chem. Phys.* **133** 124303
[20] Tian Q G, Yang J, Shi Y F, Shan X and Chen X J 2012 *J. Chem. Phys.* **136** 094306
[21] Miao Y R, Ning C G, Liu K and Deng J K 2011 *J. Chem. Phys.* **134** 204304
[22] Miao Y R, Ning C G and Deng J K 2011 *Phys. Rev. A* **83** 062706
[23] Minchinton A, Cook J P D, Weigold E and von Niessen W 1987 *Chem. Phys.* **113** 251
[24] Takahashi M, Ogino R and Udagawa Y 1998 *Chem. Phys. Lett.* **288** 714

[25] Shan X, Chen X J, Zhou L X, Li Z J, Liu T, Xue X X and Xu K Z 2006 *J. Chem. Phys.* **125** 154307
[26] Zhang Y T, Shan X, Huang C W, Zhang Z and Chen X J 2022 *J. Electron Spectrosc. Relat. Phenom.* **258** 147226
[27] Watanabe N, Chen X J and Takahashi M 2012 *Phys. Rev. Lett.* **108** 173201
[28] Wu X J, Chen X J, Chen L Q, Li Z J, Yang X F, Shan X, Zheng Y Y and Xu K Z 2005 *Chin. Phys. Lett.* **22** 1649
[29] Tian Q G, Wang K D, Shan X and Chen X J 2011 *Rev. Sci. Instrum.* **82** 033110
[30] Becke A D 1993 *J. Chem. Phys.* **98** 5648
[31] Lee C, Yang W T and Parr R G 1988 *Phys. Rev. B* **37** 785
[32] Nakatsuji H 1991 *Chem. Phys. Lett.* **177** 331
[33] Dunning T H, Jr. 1989 *J. Chem. Phys.* **90** 1007
[34] Jagutzki O, Cerezo A, Czasch A, Dorner R, Hattas M, Min H, Mergel V, Spillmann U, Ullmann-Pfleger K, Weber T, Schmidt-Bocking H and Smith G D W 2002 *IEEE Trans. Nucl. Sci.* **49** 2477
[35] Duffy P, Chong D P, Casida M E and Salahub D R 1994 *Phys. Rev. A* **50** 4707
[36] Frisch M J, Trucks G, Schlegel H B, Scuseria G E, Robb M A, Cheeseman J, Scalmani G, Barone V, Mennucci B, Petersson G A, Nakatsuji H, Caricato M, Li X, Hratchian H P, Izmaylov A F, Bloino J, Zheng G S, Sonnenberg J, Hada M and Fox D, Gaussian, Inc., Wallingford CT, 2009
[37] Duffy P, Cassida M E, Brion C E and Chong D P 1992 *Chem. Phys.* **159** 347
[38] Watanabe N, Yamazaki M and Takahashi M 2012 *J. Chem. Phys.* **137** 114301
[39] Tang Y G, Shan X, Yang J, Niu S S, Zhang Z, Watanabe N, Yamazaki M, Takahashi M and Chen X J 2016 *J. Phys. Chem. A* **120** 6855
[40] Gong M M, Zhang Y T, Li X Y, Zhang S B, Shan X and Chen X J 2022 *Phys. Rev. A* **105** 042805
[41] Zhang Y T, Gong M M, Liu Z H, Niu S S, Shan X and Chen X J 2023 *J. Phys. Chem. A* **127** 1252